frontiers in Agronomy

TYPE Original Research
PUBLISHED 26 August 2026
DOI 10.3389/fagro.2026.1923984

Check for updates

OPEN ACCESS

EDITED BY
Isabeli Pereira Bruno,
Instituto de Desenvolvimento Rural do Paraná (IDR), Brazil

REVIEWED BY
Jamshid Ali,
Beijing Forestry University, China
Soumaya Boukrouh,
Mohammed VI Polytechnic University, Morocco

*CORRESPONDENCE
Gabriella Santos Arruda de Lima
gabriella.lima@embrapa.br

†PRESENT ADDRESS
Gabriella Santos Arruda de Lima,
Brazilian Agricultural Research Corporation (Embrapa Soybean),
Londrina, Brazil

RECEIVED 30 June 2026
REVISED 29 July 2026
ACCEPTED 10 August 2026
PUBLISHED 26 August 2026

CITATION
de Lima GSA, Ferreira ME, Baumann LRF, Freitas FMC, Machado PLOA, Silva AVR, Koakuzu SN, da Silva MAS, Carvalho MTM, Santos MM and Madari BE (2026) UAV multisensor data and GAMLSS improve forage biomass estimation in Cerrado integrated crop–livestock pastures.
Front. Agron. 8:1923984.
doi: 10.3389/fagro.2026.1923984

UAV multisensor data and GAMLSS improve forage biomass estimation in Cerrado integrated crop–livestock pastures

Gabriella Santos Arruda de Lima[1*†], Manuel Eduardo Ferreira[1], Luis Rodrigo Fernandes Baumann[1], Fernanda Mara Cunha Freitas[2], Pedro Luiz Oliveira Almeida Machado[2], Antônio Vitor Resende Silva[2], Selma Nakamoto Koakuzu[2], Mellissa Ananias Soler da Silva[2], Márcia Thaís Melo Carvalho[2], Micael Moreira Santos[3] and Beata Emoke Madari[2]

[1]Remote Sensing and Geographic Information Systems (GIS) Laboratory (LAPIG), Federal University of Goiás (UFG), Goiânia, Brazil, [2]Brazilian Agricultural Research Corporation (Embrapa Rice and Beans), Santo Antônio de Goiás, Brazil, [3]Federal University of Tocantins (UFT), Palmas, Brazil

Introduction: Accurate estimation of aboveground biomass (AGB) is essential for monitoring pasture productivity and supporting sustainable management of integrated crop–livestock (ICL) systems. We hypothesized that integrating multispectral, thermal, and canopy-structural information derived from unmanned aerial vehicles (UAVs) would improve AGB prediction relative to spectral information alone, and that Generalized Additive Models for Location, Scale and Shape (GAMLSS) would accommodate seasonal heteroscedasticity while maintaining predictive performance comparable to Random Forest (RF) and Support Vector Machine (SVM) models.

Methods: We collected 280 destructive biomass samples from two ICL paddocks and one continuously grazed pasture in the Brazilian Cerrado between 2022 and 2024. Twenty-four UAV-derived predictors, including spectral bands, vegetation indices, canopy surface temperature, and canopy height, were evaluated using repeated five-fold cross-validation. Model transferability was assessed by withholding one management paddock at a time.

Results and discussion: Under repeated five-fold cross-validation, GAMLSS achieved the lowest prediction error (R^2 = 0.69 ± 0.01; RMSE = 2.15 ± 0.04 Mg ha^{-1}), followed closely by SVM (R^2 = 0.68 ± 0.01; RMSE = 2.19 ± 0.03 Mg ha^{-1}); RF showed lower accuracy (R^2 = 0.53 ± 0.01; RMSE = 2.63 ± 0.02 Mg ha^{-1}). In the paddock-transferability assessment, GAMLSS also showed the lowest error (R^2 = 0.63 ± 0.04; RMSE = 2.34 ± 0.26 Mg ha^{-1}). For GAMLSS, the complete multisensor configuration reduced RMSE by 6.2% compared with the spectral-only configuration. The selected model was used to generate spatially explicit maps of AGB and standing aboveground biomass carbon, estimated from the mean measured carbon concentration of forage biomass. Integrating multispectral, thermal, and structural UAV data with distributional regression improves AGB estimation and enables spatial monitoring of tropical pastures under contrasting management conditions.

KEYWORDS

biomass carbon stock, Cerrado, multispectral imagery, palisade grass, thermal remote sensing, tropical pasture, UAV

1 Introduction

Pastures are the predominant agricultural land use in Brazil, occupying approximately 155 million hectares and supporting livestock production across the country, particularly in the North and Central-West regions, where Urochloa spp. are widely cultivated (MapBiomas, 2025; Pedreira et al., 2015). Because pasture condition directly influences forage supply, livestock carrying capacity, land demand, degradation risk, and carbon cycling, its productive and environmental functions must be assessed jointly. Integrated crop–livestock systems (ICL) are therefore recognized as a sustainable intensification strategy that can improve soil cover, nutrient cycling, resilience, and resource-use efficiency, consistent with Brazilian low-carbon agriculture and degraded-pasture recovery policies (Cortner et al., 2019; Oliveira et al., 2018; MAPA, 2021).

Aboveground biomass (AGB) is a key indicator of forage availability, grazing capacity, pasture condition, and management efficiency. In tropical pastures, AGB varies in response to rainfall, temperature, solar radiation, soil fertility, grazing intensity, regrowth interval, and canopy development, producing strong spatial and seasonal heterogeneity. Destructive quadrat sampling provides direct and reliable biomass measurements; however, it requires intensive fieldwork, vegetation clipping, drying, and weighing, making it laborious and time-consuming when repeated over large areas or multiple sampling campaigns (Boukrouh et al., 2024). These limitations restrict the spatial and temporal frequency at which pasture biomass can be monitored.

Satellite remote sensing provides broad spatial and temporal coverage for pasture monitoring, but moderate spatial resolution, cloud contamination, and the reduced sensitivity of optical vegetation indices at high canopy density may limit the detection of within-field biomass variability (Reis et al., 2020; Santos et al., 2022, 2023). UAVs can partially overcome these limitations by acquiring centimetric-resolution spectral, thermal, and structural information. Previous studies have estimated AGB in *Brachiaria* pastures using satellite- and UAV-derived vegetation indices with machine-learning algorithms (Alvarez-Mendoza et al., 2022), combined RGB imagery and canopy height models with deep learning across contrasting pasture management conditions (Vahidi et al., 2023), and recently evaluated multispectral UAV indices in Mediterranean pastures across grazing periods and sensors (Furnitto et al., 2026). Collectively, these studies demonstrate the value of spectral and structural information but also indicate that model transferability across dates, management conditions, sensors, and environments remains a major challenge.

Random Forest (RF; Breiman, 2001) and Support Vector Machines (SVM; Cortes and Vapnik, 1995) are established nonlinear benchmarks for moderate-sized tabular datasets with correlated remote-sensing predictors and have been applied to grassland AGB estimation (Bazzo et al., 2023). However, their standard regression implementations provide point predictions without explicitly modelling response dispersion. This is relevant because residual AGB variability may differ between wet and dry seasons. GAMLSS complements these approaches by modeling both the conditional mean and dispersion of positive, potentially skewed AGB distributions, with season included as a predictor of dispersion (Rigby and Stasinopoulos, 2005). Thus, RF and SVM served as predictive benchmarks, whereas GAMLSS addressed the distributional component of the analysis.

Despite recent advances, the most closely related studies have either combined vegetation indices with machine-learning models, integrated RGB imagery and canopy height with deep-learning approaches, or evaluated multispectral UAV indices across grazing periods and sensors. To the best of our knowledge, no previous study has jointly evaluated multispectral reflectance, canopy surface temperature, and photogrammetric canopy height using a distributional regression framework that models both the conditional mean and season-dependent dispersion of AGB in tropical pastures under ICL and continuous grazing, while also comparing observation-level predictive performance with leave-one-paddock-out transferability. This combination is agronomically relevant because wet–dry seasonality, grazing pressure, senescence, exposed soil, and non-photosynthetic vegetation may alter not only mean AGB but also its variability and the spectral, thermal, and structural response of the canopy. Spatially explicit AGB estimates may also be converted into standing aboveground biomass carbon; however, this represents only one ecosystem carbon pool and should not, in isolation, be interpreted as evidence of net carbon sequestration or carbon-credit generation.

Accordingly, this study aimed to: (1) integrate multispectral, thermal, and structural variables obtained from UAV surveys to estimate pasture AGB under ICL and continuous pasture systems; (2) compare RF, SVM, and GAMLSS under validation approaches designed to assess both observation-level predictive accuracy and transferability among paddocks with contrasting management conditions; and (3) produce spatially explicit maps of AGB and standing aboveground biomass carbon under contrasting pasture conditions. We tested three hypotheses: H1, adding thermal and structural predictors to spectral variables reduces AGB prediction error relative to spectral-only models; H2, GAMLSS explicitly represents season-dependent heteroscedasticity while maintaining predictive performance comparable to RF and SVM; H3, model transferability declines across paddocks with contrasting management conditions.

2 Materials and methods

2.1 Study area

The study area is located at Capivara Farm Platform, owned by the National Rice and Beans Research Centre of the Brazilian Agricultural Research Corporation (Embrapa Rice and Beans) (Figure 1), in the municipality of Santo Antônio de Goiás, Brazil. The area is also a Technological and Research Reference Unit (URTP) of the ILPF Network (Associação Rede ILPF: a public-private partnership to promote crop-livestock-forestry throughout Brazil, https://redeilpf.org.br/#). Since the 2003/2004 crop season, the Capivara Farm Platform has been managed under an integrated crop–livestock system (ICL) heavily monitored. The URTP consists of two paddocks under ICL: the first identified as “C4”, with 7.45 ha, and the second as “C5”, with 8.00 ha. In addition to these, there is a third paddock (C6), under continuous pasture (5.04 ha), considered degraded, with the presence of termite mounds, invasive plants, and some patches of bare soil, used here as a baseline. Another baseline is a forest adjacent to the ICL areas, characterized by the phytophysiognomic type Semideciduous Dry Forest, covering approximately 300 ha and representing the Legal Reserve (LR) area. A detailed description of the URTP paddocks is provided in Oliveira et al. (2022). The land use and management of the areas during the years evaluated in this study are presented in Table 1.

This study was divided into four stages: field and laboratory work (Section 2.2), image processing (Section 2.3), model development and evaluation (Section 2.4), and mapping of AGB and the corresponding carbon stock (Section 2.5).

2.2 Field and laboratory work

Biomass sampling was conducted during the pasture phase of the integrated crop–livestock paddocks C4 and C5 and the continuous pasture paddock C6 from November 2022 to February 2024, covering both the dry and rainy seasons. Field sampling was conducted concurrently with UAV image acquisition. Twenty biomass sampling points were evaluated in each experimental paddock during each campaign, resulting in 14 paddock–campaign combinations and a total of 280 observations used for model development and evaluation. The temporal distribution of the sampling campaigns, the experimental paddocks evaluated, and the corresponding number of biomass samples are summarized in Table 2.

Sampling locations were newly selected during each field campaign; therefore, the same physical locations were not repeatedly sampled over time. This procedure was necessary because biomass collection was destructive and prevented subsequent measurements at the exact harvested locations. Consequently, the observations represented distinct physical sampling units nested within each paddock and campaign rather than repeated measurements of the same quadrats. Nevertheless, observations collected within the same paddock–campaign combination shared common environmental, management, and UAV image-acquisition conditions.

At each sampling point, canopy height was measured using a graduated ruler positioned at the curvature of the upper leaves,

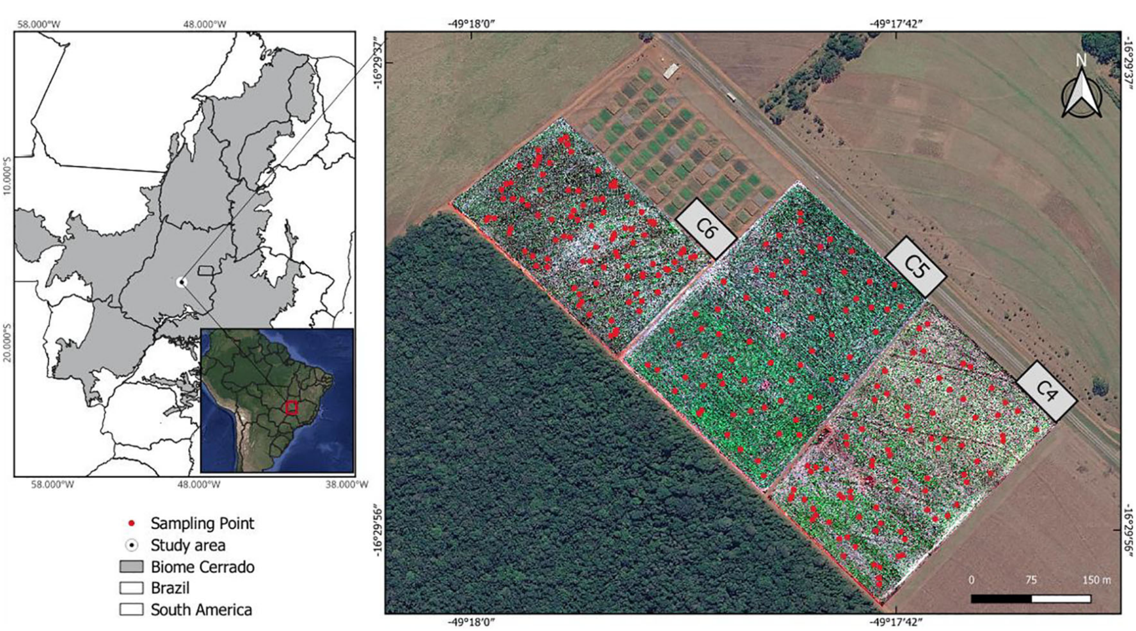

FIGURE 1
Location of the Capivara Farm platform and distribution of sampling points for biomass measurement in integrated crop-livestock (ICL; C4 and C5) and continuous pasture (C6) of Embrapa Rice and Beans in Santo Antônio de Goiás, Goiás State, Brazil. The permanent set-aside area (Legal Reserve) is the large dark area on the left side of the image.

TABLE 1 Land use and management history of study paddocks C4 and C5 under integrated crop–livestock systems (ICL) at Capivara Farm Platform, Embrapa Rice and Beans, Santo Antônio de Goiás, Goiás State, Brazil, during the study period (2022–2024).

Growing season	ICL paddock			
	C4		C5	
	Summer	Winter	Summer	Winter
2022/2023	U(P)[1]	U(P)[1]	Common bean[2]/ rainfed rice[3] + U(P)[1], NT[4]	U(P)[1]
2023/2024	U(P)[1]	U(P)[1]	Rainfed rice[3] + U(P)[1], NT[4]	U(P)[1]

[1]U(P), palisade grass (*Urochloa brizantha*) cultivar BRS Paiaguás cultivated as pasture; [2]Common bean (*Phaseolus vulgaris*) cultivar BRS FC104; [3]Rainfed rice (*Oryza sativa*) cultivar BRS A501 CL; [4]NT, no-tillage system. Summer: November to April, rainy season; Winter: May to October, dry season.

following Frame (1981). The standing aboveground biomass of the cultivated forage was then harvested at ground level within a 0.5 × 0.5 m quadrat. Each sampling point was individually georeferenced using geodetic-grade GNSS receivers to enable spatial correspondence with the UAV-derived imagery (Supplementary Material). Only the aboveground tissues of the cultivated forage were included, whereas roots, litter, weeds, and other non-forage species were excluded.

The harvested material was weighed fresh, and a subsample was dried in a forced-air oven at 55°C for 72 h, or until constant weight, to determine dry aboveground biomass, expressed in Mg ha^{-1}. An aliquot of the dried biomass was analyzed for total carbon concentration (%) using a PerkinElmer 2400 Series II CHNS/O elemental analyzer (Nelson and Sommers, 1996). Aboveground biomass carbon stock (Mg ha^{-1}) was subsequently calculated by multiplying dry AGB by the corresponding carbon concentration. Results are expressed as the variability of C concentration and stocks only for the cultivated *U. brizantha* (cv. BRS Paiaguas) between seasons (rainy and dry), regardless of paddock sample (C4, C5 and C6).

TABLE 2 Distribution of aboveground biomass (AGB) samples across sampling campaigns and experimental paddocks.

Sampling month	Season	Study paddocks sampled	Number of biomass samples
November 2022	Rainy	C6	20
December 2022	Rainy	C4	20
March 2023	Rainy	C4 and C6	40
May 2023	Dry	C6	20
June 2023	Dry	C4, C5, and C6	60
September 2023	Dry	C4, C5, and C6	60
December 2023	Rainy	C4	20
February 2024*	Rainy	C4 and C6	40
Overall total		14 paddock–campaign combinations	280 samples

C4 and C5 correspond to integrated crop–livestock (ICL) paddocks, whereas C6 corresponds to the paddock under continuous pasture. The C4 and C6 samples listed for *February 2024 were collected in separate campaigns within the same month.
Twenty biomass samples were collected per paddock in each campaign.

2.3 UAV image acquisition and processing

Fifteen ground control points (GCPs) were established and strategically distributed around and within the three study areas (Figure 1). These points were georeferenced using a pair of geodetic GNSS receivers (Topcon Hiper Lite+) operating in post-processed kinematic (PPK) mode, with corrections from the IBGE geodetic station network within the Brazilian Geodetic System (SGB). The use of GCPs optimized the geometry of the orthomosaics and ensured centimetre-level accuracy for the aerophotogrammetric products generated in the experiment.

Image acquisition was performed using a rotary-wing UAV (quadcopter), a DJI Matrice 200, equipped with a MicaSense Altum multispectral sensor coupled to a Downwelling Light Sensor (DLS) for radiometric correction. The sensor has five bands distributed across the visible, red-edge, and near-infrared regions of the spectrum, with band centres at approximately 475 nm (blue), 560 nm (green), 668 nm (red), 717 nm (red edge), and 842 nm (near-infrared, NIR), in addition to a thermal long-wave infrared (LWIR) sensor centred at 11, 000 nm.

Flights were conducted at an altitude of 90 m above ground level, with 70% frontal and lateral overlap, resulting in a ground sampling distance (GSD) of approximately 5 cm pixel^{-1}. Image acquisition was performed between 10:00 a.m. and 1:00 p.m. from November 2022 to February 2024 (Figure 2), under clear-sky conditions and stable illumination. This time window was selected to standardize acquisitions near solar noon, reduce variations in solar angle and shadowing, and improve the comparability of spectral and thermal measurements across campaigns. Wind speed was not systematically recorded or controlled and was not included as a flight-selection criterion or modelling variable. Before each flight, images of a grayscale calibration panel with known reflectance values were acquired and subsequently used for radiometric correction, allowing illumination conditions to be normalized across acquisition dates.

Image processing was carried out in Pix4Dmapper software (version 4.4.12, Pix4D SA, Lausanne, Switzerland), following a standard photogrammetric workflow that included image alignment, dense point cloud generation, and block adjustment with incorporation of the GCPs. From these products, digital surface models (DSMs), digital terrain models (DTMs), and reflectance-calibrated orthomosaics were generated, all projected in the WGS 1984 UTM Zone 22S coordinate system.

The canopy height model (CHM) was calculated as the difference between the digital surface model (DSM) and the digital terrain model (DTM). The DSM and DTM were used exclusively to derive the CHM and were not included as independent predictors in the models. The final predictor set comprised 24 variables: five reflectance bands and one thermal band blue, green, red, red edge, near-infrared, and thermal, 17 vegetation indices derived from the spectral bands (Table 3), and one structural variable represented

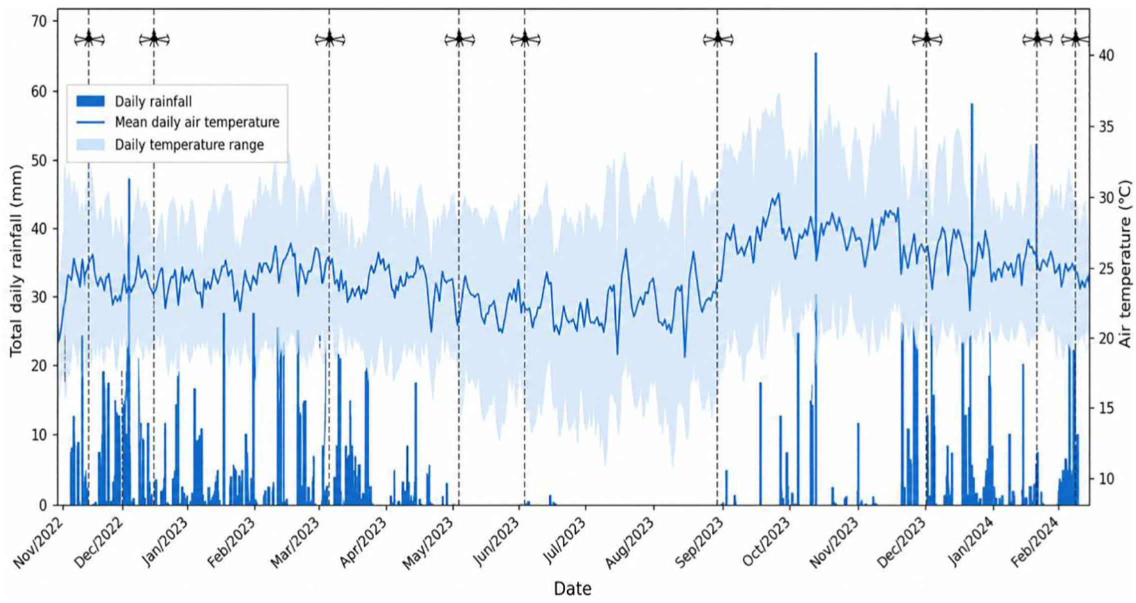

FIGURE 2
Local daily meteorological data: air temperature and rainfall conditions during the 2022–2024 UAV flight campaigns conducted in the integrated crop-livestock system (ICL: areas C4 and C5), continuous pasture (C6) and the permanent set-aside area (Legal Reserve) in Santo Antônio de Goiás, GO, Brazil. Dashed vertical lines and UAV icons indicate the dates of image acquisition used for biomass sampling and pasture monitoring.

by the CHM. For each biomass sampling point, mean pixel values of the 24 predictor variables were extracted from the corresponding sampling area in the UAV-derived imagery. The vegetation indices were selected to represent complementary canopy properties, including greenness and biomass-related variation, chlorophyll and red-edge responses, sensitivity to soil background, and visible-band responses associated with senescence, non-photosynthetic vegetation, and bare soil.

2.4 Model development and evaluation

Aboveground biomass (AGB) was modelled using three approaches: RF, SVM, and GAMLSS. RF and SVM were selected as nonlinear machine-learning benchmarks, whereas GAMLSS was used to model the positive, asymmetric, and potentially heteroscedastic distribution of AGB. All 280 field observations described in Section 2.2 were included in model development

TABLE 3 Vegetation index formulas used in this study.

Vegetation index	Abbreviation	Formula	Reference
Green Chlorophyll Index	CIgreen	$(\rho_{NIR}/\rho_{GREEN}) - 1$	Gitelson et al., 2003
Chlorophyll Vegetation Index	CVI	$(\rho_{NIR} \times \rho_{RED})/\rho_{GREEN}^2$	Vincini et al., 2008
Enhanced Vegetation Index	EVI	$2.5 \times (\rho_{NIR} - \rho_{RED})/(\rho_{NIR} + 6\rho_{RED} - 7.5\rho_{BLUE} + 1)$	Huete et al., 2002
Excess Green Index	ExG	$2\rho_{GREEN} - \rho_{RED} - \rho_{BLUE}$	Woebbecke et al., 1995
Green Leaf Index	GLI	$(2\rho_{GREEN} - \rho_{RED} - \rho_{BLUE})/(2\rho_{GREEN} + \rho_{RED} + \rho_{BLUE})$	Louhaichi et al., 2001
Green Normalized Difference Vegetation Index	GNDVI	$(\rho_{NIR} - \rho_{GREEN})/(\rho_{NIR} + \rho_{GREEN})$	Gitelson et al., 1996
Intensity Index	Intensity	$(1/30.5) \times (\rho_{RED} + \rho_{GREEN} + \rho_{BLUE})$	Escadafal et al., 1994
Modified Photochemical Reflectance Index	MPRI	$(\rho_{GREEN} - \rho_{RED})/(\rho_{GREEN} + \rho_{RED})$	Yang et al., 2008
MERIS Terrestrial Chlorophyll Index	MTCI	$(\rho_{NIR} - \rho_{RE})/(\rho_{RE} - \rho_{RED})$	Dash and Curran, 2004
Normalized Difference Red-Edge Index	NDRE	$(\rho_{NIR} - \rho_{RE})/(\rho_{NIR} + \rho_{RE})$	Fitzgerald et al., 2006
Normalized Difference Vegetation Index	NDVI	$(\rho_{NIR} - \rho_{RED})/(\rho_{NIR} + \rho_{RED})$	Rouse et al., 1974
Normalized Difference Red-Edge/Red Index	NDVIre	$(\rho_{RE} - \rho_{RED})/(\rho_{RE} + \rho_{RED})$	Gitelson and Merzlyak, 1994
Soil-Adjusted Vegetation Index	SAVI	$[(1 + L) \times (\rho_{NIR} - \rho_{RED})]/(\rho_{NIR} + \rho_{RED} + L)$	Huete, 1988
Triangular Greenness Index	TGI	$\rho_{GREEN} - 0.39\rho_{RED} - 0.61\rho_{BLUE}$	Hunt et al., 2011
Triangular Vegetation Index	TVI	$0.5 \times [120(\rho_{NIR} - \rho_{GREEN}) - 200(\rho_{RED} - \rho_{GREEN})]$	Broge and Leblanc, 2001
Visible Atmospherically Resistant Index	VARI	$(\rho_{GREEN} - \rho_{RED})/(\rho_{GREEN} + \rho_{RED} - \rho_{BLUE})$	Gitelson et al., 2002
Wide Dynamic Range Vegetation Index	WDRVI	$(0.2\rho_{NIR} - \rho_{RED})/(0.2\rho_{NIR} + \rho_{RED})$	Gitelson, 2004

ρ denotes reflectance; BLUE, GREEN, RED, RE, and NIR denote the blue, green, red, red-edge, and near-infrared bands, respectively. For SAVI, L = 0.5. For WDRVI, α = 0.2.

and evaluation. All statistical modelling and computational analyses were performed in R software version 4.5.2 (R Core Team, 2025), utilizing the data.table, caret, randomForest, e1071, gamlss, and gamlss.dist packages.

2.4.1 Predictor variables and model development

The complete predictor set comprised the 24 UAV-derived variables described in Section 2.3 and Table 3: five spectral reflectance bands, 17 vegetation indices, canopy surface temperature (TEMP), and the canopy height model (CHM). These variables represented complementary spectral, thermal, and structural information related to pasture AGB.

Four predictor configurations were evaluated to quantify the incremental contribution of thermal and structural information: spectral predictors only (S); spectral predictors plus canopy surface temperature (S + TEMP); spectral predictors plus the canopy height model (S + CHM); and the complete multisensor configuration, comprising spectral predictors, TEMP, and CHM (S + TEMP + CHM).

TEMP represented the thermal predictor, whereas CHM represented the structural predictor. The digital surface model and digital terrain model were used only to derive CHM and were not included as independent predictors.

Before model fitting, the dataset was checked for missing, non-finite, and non-positive AGB values. No imputation was performed. All analyses required complete observations with finite predictor values, and AGB was required to be strictly positive because a Gamma response distribution was used for GAMLSS.

To avoid information leakage, predictor filtering and standardization were repeated separately within every training subset created by the validation procedures. Spectral predictors with zero or near-zero variance were first removed using the nearZeroVar function. Pairwise correlations were then calculated among the remaining spectral predictors. When the absolute correlation between two predictors exceeded 0.95, the findCorrelation algorithm, with exact = TRUE, removed the predictor with the greater mean absolute correlation with the remaining predictor set. TEMP and CHM were not subjected to correlation-based filtering, but they were removed from a configuration when they had zero variance in the corresponding training subset.

The retained predictors were centred and scaled using means and standard deviations calculated only from the training data. These same parameters were then applied to the held-out observations. For each validation split, RF, SVM, and GAMLSS used the same training and test observations and the same retained predictor set, allowing direct comparison under equivalent conditions.

2.4.2 Random forest

RF models were fitted using the randomForest package with 500 regression trees. The number of predictors randomly considered at each split (mtry) was tuned within each external training set using internal three-fold cross-validation. Candidate values corresponded approximately to √p, p/4, p/3, p/2, and p, where p was the number of predictors retained in that training set. The value producing the lowest internal RMSE was selected. MAE and, subsequently, the smaller mtry value were used as tie-breaking criteria. The minimum terminal node size was five observations. No maximum number of terminal nodes was imposed, and no post-pruning was applied.

RF performance was evaluated using two external validation schemes. First, repeated five-fold cross-validation was used to assess observation-level predictive performance within the dataset. In each repetition, the 280 observations were divided into five folds. Four folds were used for training (n=224), and the remaining fold was used for testing (n=56). The complete five-fold procedure was repeated ten times, resulting in 50 external training–test evaluations. Within each external training set, predictor filtering, standardization, and mtry tuning were completed before predictions were generated for the held-out fold.

Second, leave-one-paddock-out validation was used to assess the model's ability to predict an unseen management paddock within the same experimental farm. Paddocks C4, C5, and C6 were excluded one at a time and used exclusively for testing. When C4 or C6 was excluded, 160 observations were used for training and 120 for testing. When C5 was excluded, 240 observations were used for training and 40 for testing. All predictor preprocessing and mtry tuning were performed using only observations from the two retained paddocks.

Repeated five-fold cross-validation represented within-dataset predictive performance because observations from the same paddock or sampling campaign could occur in both the training and test folds. Leave-one-paddock-out validation represented transferability to an unseen paddock within the same experimental farm and was not considered validation across independent farms, regions, or environmental conditions.

2.4.3 Support vector machine

SVM models were fitted as epsilon-support vector regressions with a radial basis function kernel using the e1071 package. Cost and gamma were tuned within each training subset by three-fold cross-validation. Candidate cost values were 2^{-1}, 2^{0}, 2^{1}, 2^{2}, 2^{3}, and 2^{4}. Candidate gamma values were 0.25/p, 0.5/p, 1/p, 2/p, and 4/p, where p was the number of retained predictors. The cost-gamma combination with the lowest internal RMSE was selected, with MAE used as a secondary criterion. Because predictors were standardized before model fitting, additional scaling within the SVM function was disabled. Epsilon was not tuned and was retained at the package default value of 0.1.

SVM performance was evaluated using the same two validation schemes. In repeated five-fold cross-validation, each model was trained with 224 observations and tested with 56 observations in each fold. The five-fold procedure was repeated ten times, resulting in 50 evaluations. Predictor filtering, standardization, and cost-gamma tuning were performed separately within each training set before the held-out fold was predicted.

In leave-one-paddock-out validation, one complete paddock was excluded at a time. C4 and C6 were each evaluated using 160 training and 120 test observations, whereas C5 was evaluated using 240 training and 40 test observations. The excluded paddock was not used during preprocessing, hyperparameter tuning, or model fitting. Repeated five-fold cross-validation was used to assess within-dataset predictive performance, whereas leave-one-paddock-out validation was used to assess transferability among paddocks within the same experimental farm.

2.4.4 GAMLSS

Before model validation, candidate response distributions for positive continuous data were screened using the fitDist function from the gamlss package with type = "realplus". Distributions were ranked using the generalized Akaike information criterion (GAIC) with k = 2. The Gamma distribution (GA) produced the lowest GAIC and was therefore selected for the subsequent GAMLSS analyses. This choice was also consistent with the continuous, strictly positive, and right-skewed distribution of AGB.

The conditional mean parameter (μ) was modelled from the retained UAV-derived predictors using Ridge-penalized regression through the ri() function, with Lp = 2. The Ridge penalty was estimated by maximum likelihood separately within each training subset. The dispersion parameter (σ) was modelled as a function of season so that conditional AGB variability could differ between the rainy and dry periods. Season was included only in the dispersion submodel and not as a predictor of the conditional mean. No nonparametric smoothing terms were used, and logarithmic link functions were adopted for both μ and σ.

$$\mathrm{AGB_i} \sim \mathrm{GA}(\mu_i, \sigma_i)$$

$$\log(\mu_i) = \beta_0 + \mathrm{ri}(X_i,\ L_p = 2,\ \mathrm{method} = \text{"ML"})$$

$$\log(\sigma_i) = \gamma_0 + \gamma_1\ \mathrm{Season_i}$$

where X_i denotes the predictor set retained in the corresponding training subset. Models were fitted using the gamlss and gamlss.dist packages, with a maximum of 300 fitting cycles. AGB predictions were obtained on the response scale from the fitted conditional mean, μ.

GAMLSS performance was evaluated using the same repeated five-fold and leave-one-paddock-out schemes. In repeated five-fold cross-validation, 224 observations were used for training, and 56 for testing in each fold, and the complete procedure was repeated ten times. Predictor filtering, standardization, ridge-penalty estimation, and estimation of the mean and dispersion parameters were performed only with the training observations before the held-out fold was predicted.

In leave-one-paddock-out validation, C4, C5, and C6 were excluded one at a time. The corresponding training-test sizes were 160–120 for C4, 240–40 for C5, and 160–120 for C6. The excluded paddock did not contribute to predictor filtering, standardization, ridge-penalty estimation, or model fitting.

The season-dependent dispersion specification (σ ~ season) was also compared with a constant-dispersion model (σ ~ 1). Both models used the same Gamma family and conditional-mean specification. Their fit was compared using the Akaike information criterion and a likelihood-ratio test. The fitted μ and σ parameters were used to derive 95% distributional prediction intervals from the 0.025 and 0.975 quantiles of the fitted Gamma distribution.

2.4.5 Contribution of thermal and structural predictors

For each modelling approach, the contribution of thermal and structural information was evaluated by comparing the RMSE of the S + TEMP, S + CHM, and S + TEMP + CHM configurations with the RMSE of the spectral-only configuration. The relative reduction in RMSE was calculated as:

$$\mathrm{RMSE\ reduction}\ (\%) = 100 \times [(\mathrm{RMSE_s} - \mathrm{RMSE_j})/\mathrm{RMSE_s}]$$

where RMSE_S is the prediction error of the spectral-only configuration, and RMSE_j is the error of the evaluated configuration. Positive values indicate lower prediction error than the spectral-only model, whereas negative values indicate higher prediction error.

2.4.6 Performance metrics

Predictive performance was quantified using the cross-validated coefficient of determination (R^2pred), root mean square error (RMSE), mean absolute error (MAE) (Equations 1-4), and prediction bias:

$$R^2 = 1 - \frac{\sum_{i=1}^{n}(y_i - \hat{y}_i)^2}{\sum_{i=1}^{n}(y_i - \underline{y_i})^2} \tag{1}$$

$$RMSE = \sqrt{\frac{\sum_{i=1}^{n}(y_i - \hat{y}_i)^2}{n}} \tag{2}$$

$$MAE = \frac{1}{n}\sum_{i=1}^{n}|y_i - \hat{y}_i| \tag{3}$$

$$Bias = \frac{1}{n}\sum_{i=1}^{n}(\hat{y}_i - y_i) \tag{4}$$

where y_i is the observed AGB, $\hat{y}_i$ is the corresponding held-out prediction, $\bar{y}$ is the mean observed AGB in the evaluated data, and n is the number of evaluated observations. Negative bias indicates overall underestimation, whereas positive bias indicates overestimation. Differences among RF, SVM, and GAMLSS were interpreted descriptively because no formal paired statistical comparison of prediction errors was performed.

For repeated five-fold cross-validation, metrics were calculated from held-out predictions and summarized as the mean and standard deviation across the ten repetitions. For leave-one-paddock-out validation, results were summarized as the mean and standard deviation across the three excluded paddocks.

2.5 AGB and biomass carbon mapping

After completion of all validation analyses, the model–predictor configuration with the lowest numerical mean RMSE under leave-one-paddock-out validation was selected for spatial prediction. The selected specification was subsequently refitted using all 280 field observations. Predictor filtering and standardization were repeated using the complete dataset, and the resulting preprocessing parameters were applied to the corresponding raster predictors.

The selected model was applied to the spatially continuous predictor rasters to generate pixel-level AGB estimates for each study paddock. Before prediction, all predictor layers were resampled and aligned to a common spatial extent, coordinate reference system, and pixel grid. Pixels containing missing predictor values or representing areas outside the evaluated pasture areas were excluded from the predictions.

Aboveground biomass carbon was calculated from predicted AGB using the mean measured carbon concentration of the dry matter (0.42 ± 0.01 g C g^{-1}). The same value of the carbon concentration was therefore applied to all predicted pixels:

$$\text{Aboveground biomass carbon} = \text{Predicted AGB} \times \text{carbon concentration}$$

Where aboveground biomass carbon stock is expressed in Mg C ha^{-1}, and predicted AGB is expressed in Mg dry matter ha^{-1}.

The resulting AGB and AGB carbon rasters were processed and displayed in QGIS version 3.30. The maps represent the spatial distribution of standing forage biomass and its associated aboveground biomass carbon stock at the time of the corresponding UAV survey. They do not represent net carbon sequestration, total ecosystem carbon stocks, or changes in carbon storage over time. The final maps were generated with a pixel size of 0.05 m.

3 Results

3.1 Statistical analysis of field variables and spectral bands

Figure 3; Table 4 summarize the seasonal variation in field-measured AGB and canopy height. Compared to the dry season, both variables were significantly higher during the rainy season. Rainy-season AGB was 26.5% higher than dry-season AGB, corresponding to a moderate effect size. Canopy height decreased by 44.2% from the rainy to the dry season, corresponding to a very large effect size. On the other hand, measured carbon concentration in AGB was virtually identical in the rainy and dry seasons, at 42.2 g C kg^{-1} dry matter in both cases, and this was reflected in the biomass carbon stocks in the rainy (0.32 ± 0.08 Mg C ha^{-1}; n = 60) and in the dry seasons (0.29 ± 0.14 Mg C ha^{-1}; n = 140), which did not differ significantly (Welch's test, t = 1.53, df = 176, p > 0.1).

At the paddock level, C4 descriptively exhibited the highest AGB and canopy height values and the widest distributions, particularly following animal exclusion and pasture regrowth. In contrast, C6, which was maintained under continuous grazing, showed lower central values and a narrower range of variation. Paddock C5 was not represented during the rainy season because the area was occupied by annual crops during that period. These paddock-level patterns should be interpreted descriptively because no formal statistical comparison among management systems was performed.

Figure 4 summarizes the seasonal variation in spectral reflectance and canopy temperature derived from UAV imagery. During the dry season, reflectance increased in the visible bands, particularly in the RED band, whereas NIR and red-edge reflectance were higher during the rainy season. Mean NIR reflectance decreased from approximately 0.39 in the rainy season to 0.28 in the dry season, while mean canopy temperature increased from about 30°C to more than 32°C. Maximum temperatures exceeded 39°C during the dry season but remained close to 34°C during the rainy season. Greater dispersion in the visible bands and temperature was also observed during the dry season, indicating increased spectral and thermal heterogeneity.

3.2 Model performance

Model performance under observation-level repeated five-fold cross-validation and paddock-level leave-one-paddock-out validation is summarized in Table 5. Under repeated five-fold cross-validation, GAMLSS yielded the lowest numerical prediction errors (R^2pred = 0.69 ± 0.01, RMSE = 2.15 ± 0.04 Mg ha^{-1}, and MAE = 1.72 ± 0.03 Mg ha^{-1}), followed closely by SVM. Random Forest showed lower predictive accuracy, with R^2pred = 0.53 ± 0.01 and RMSE = 2.63 ± 0.02 Mg ha^{-1}.

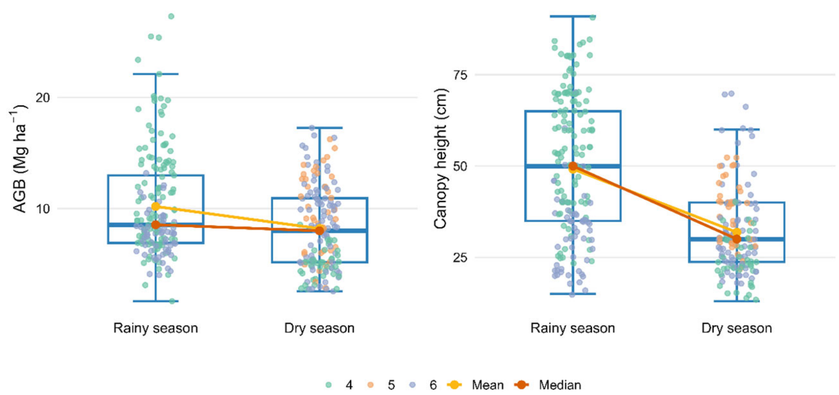

FIGURE 3
Seasonal variation in aboveground biomass (AGB) and canopy height under rainy- and dry-season conditions. Box-and-whisker plots show the distribution of field measurements obtained in the integrated crop–livestock paddocks C4 and C5 and the continuous pasture paddock C6. The dataset comprised 140 observations from rainy-season campaigns and 140 observations from dry-season campaigns.

TABLE 4 **Seasonal differences in aboveground biomass and canopy height based on Welch's t-tests.**

Variable	Rainy season mean ± SD	Dry season mean ± SD	Mean difference	Welch's t-test, t (df)	p-value	95% CI	Cohen's d
AGB (Mg ha^{-1})	10.11 ± 4.67	7.99 ± 3.83	2.12	4.15 (267.74)	p < 0.001	1.11–3.12	0.53
Canopy height (cm)	55.76 ± 17.88	31.09 ± 11.15	24.66	13.85 (232.92)	p < 0.001	21.15–28.17	1.65

Prediction accuracy decreased when entire paddocks were excluded from model fitting. Under leave-one-paddock-out validation, GAMLSS retained the lowest numerical RMSE and MAE, followed by SVM and Random Forest. Relative to repeated five-fold cross-validation, RMSE increased by 8.8% for GAMLSS, 4.2% for Random Forest, and 12.3% for SVM. These results show that transferring predictions to a paddock not represented during model fitting was more challenging than predicting randomly withheld observations. Because no formal paired statistical comparison among model errors was performed, differences among algorithms are interpreted as numerical rather than statistically significant evidence of model superiority.

Figure 5 presents the relationship between observed and predicted AGB under leave-one-paddock-out validation. Predictions from all three models generally followed the observed variation in AGB, but deviations from the 1:1 line increased at higher biomass values. GAMLSS showed the closest overall numerical agreement with the 1:1 relationship, whereas SVM showed intermediate agreement. Random Forest produced the strongest compression of the predicted range and the most pronounced underestimation of high-AGB observations. This pattern indicates that all models had greater difficulty representing the upper tail of the biomass distribution when predictions were transferred to an excluded paddock. The shaded areas represent 95% confidence bands around the fitted observed–predicted relationships and should not be interpreted as the distributional prediction intervals generated by GAMLSS.

The contribution of canopy surface temperature and CHM to AGB prediction under leave-one-paddock-out validation was model-dependent (Figure 6). Values were expressed as percentage changes in RMSE relative to the spectral-only configuration and summarized across the three paddock exclusions. For GAMLSS, adding canopy surface temperature reduced RMSE by 5.3%, whereas adding CHM reduced RMSE by 2.2%. The complete multisensor configuration produced the largest improvement for GAMLSS, reducing RMSE by 6.2%. Random Forest showed comparatively small gains, with RMSE reductions ranging from 0.6% to 2.1%. The largest reduction was obtained with the addition of TEMP alone, whereas the complete TEMP+CHM configuration produced a smaller improvement, indicating that the contribution of the additional structural predictor was not cumulative. In contrast, the inclusion of thermal and structural predictors increased SVM prediction error, with the complete multisensor configuration increasing RMSE by 9.0%.

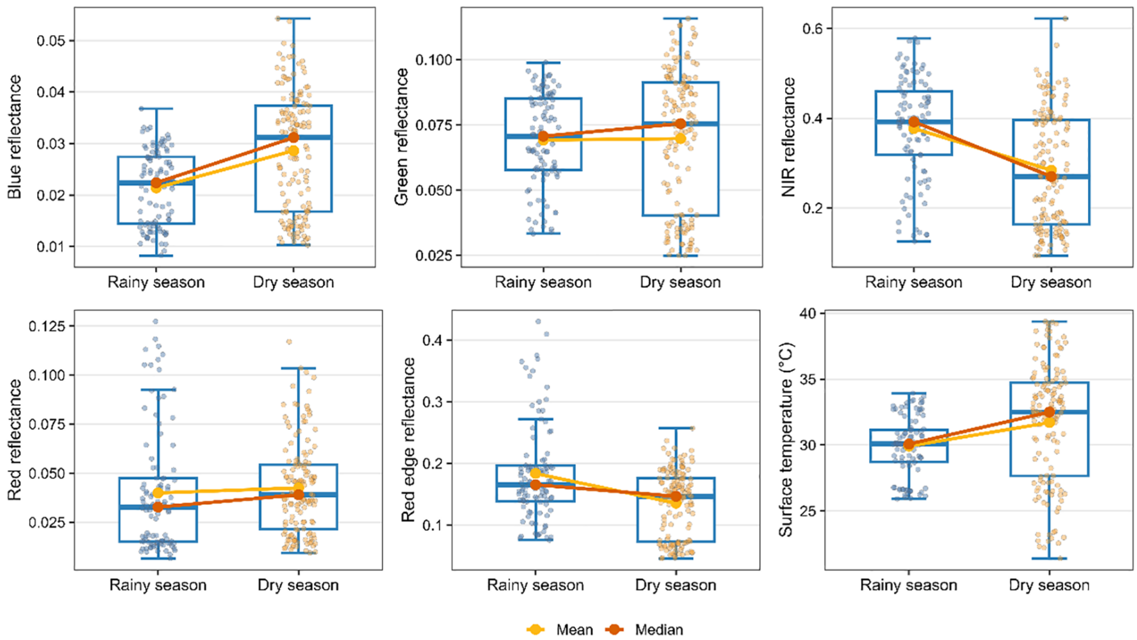

FIGURE 4
Seasonal variation in spectral reflectance bands and canopy surface temperature under rainy- and dry-season conditions. Box-and-whisker paddocks show the distribution of UAV-derived measurements obtained in the integrated crop–livestock paddocks C4 and C5 and the continuous pasture paddock C6. The dataset comprised 140 observations from rainy-season campaigns and 140 observations from dry-season campaigns.

TABLE 5 Predictive AGB (Mg ha^{-1}) performance of GAMLSS, random forest, and radial support vector machine under observation-level repeated 5-fold cross-validation and paddock-level leave-one-paddock-out validation.

Validation scheme	Model	R^2pred	RMSE (Mg ha^{-1})	MAE (Mg ha^{-1})	Bias (Mg ha^{-1})	RMSE change (Mg ha^{-1}; %)
Observation-level interpolation (Repeated 5-fold cross-validation)	GAMLSS	0.69 ± 0.01	2.15 ± 0.04	1.72 ± 0.03	0.02 ± 0.02	—
	Random Forest	0.53 ± 0.01	2.63 ± 0.02	2.11 ± 0.02	0.02 ± 0.02	—
	SVM Radial	0.68 ± 0.01	2.19 ± 0.03	1.75 ± 0.02	−0.06 ± 0.03	—
Paddock-level transferability (Leave-one-paddock-out validation)	GAMLSS	0.63 ± 0.04	2.34 ± 0.26	1.87 ± 0.07	−0.05 ± 0.69	+0.19 (+8.8%)
	Random Forest	0.49 ± 0.02	2.74 ± 0.36	2.15 ± 0.22	−0.18 ± 0.70	+0.11 (+4.2%)
	SVM Radial	0.59 ± 0.10	2.46 ± 0.17	1.89 ± 0.04	−0.28 ± 0.44	+0.27 (+12.3%)

R^2pred, cross-validated coefficient of determination; RMSE, root mean square error; MAE, mean absolute error. Bias was calculated as predicted minus observed AGB; therefore, negative values indicate overall underestimation. RMSE change was calculated relative to repeated 5-fold cross-validation, with positive values indicating increased prediction error under leave-one-paddock-out validation.

The final GAMLSS model accounted for seasonal heteroscedasticity by allowing the dispersion parameter, σ, to vary across seasons (Figure 7). Across the resampling folds, mean dispersion was lower during the rainy season, approximately 0.19, and increased to approximately 0.30 during the dry season. This pattern indicates greater conditional relative variability in AGB during the dry season, even after accounting for the spectral, thermal, and structural predictors included in the model.

In the models fitted to the complete dataset, allowing dispersion to vary by season improved model fit relative to the constant-dispersion formulation (AIC = 1200.50 versus 1214.64; ΔAIC = 14.14; likelihood-ratio χ^2 = 16.10, df = 1, p = 5.78 × 10^{-5}). These results support the use of a distributional framework in which seasonal differences are represented not only in expected biomass but also in its conditional variability.

3.3 Spatial distribution of predicted biomass and aboveground biomass carbon

After completion of the validation procedures, the final Gamma GAMLSS model using the complete multisensor predictor configuration was refitted with all 280 field observations and applied pixel by pixel to the aligned UAV-derived raster predictors. The resulting spatial products represent conditional mean predictions of standing aboveground biomass for the dates of the corresponding UAV surveys. Aboveground biomass carbon stock was estimated by applying the mean carbon concentration measured in the dry matter of the palisade grass (0.42 ± 0.01 g C g^{-1}) uniformly to all pixels, paddocks, and sampling seasons. Therefore, the carbon-stock maps directly reflect the spatial patterns of GAMLSS-predicted biomass rather than predictions from an independently fitted carbon model. Figure 8 shows the spatial distribution of predicted aboveground biomass and the corresponding standing aboveground biomass carbon stock for the dry- and rainy-season surveys in the integrated crop–livestock paddocks C4 and C5 and the continuous pasture in the paddock C6. Paddock C5 is not shown in the rainy-season map because it was under the crop phase (rainfed rice) of the integrated system.

For the paddocks under both seasonal conditions, particularly C4 and C6, predicted AGB and aboveground biomass carbon stock were generally higher during the rainy-season surveys and lower during the dry-season surveys. During the dry-season surveys, C5 showed comparatively high predicted AGB and carbon stock in

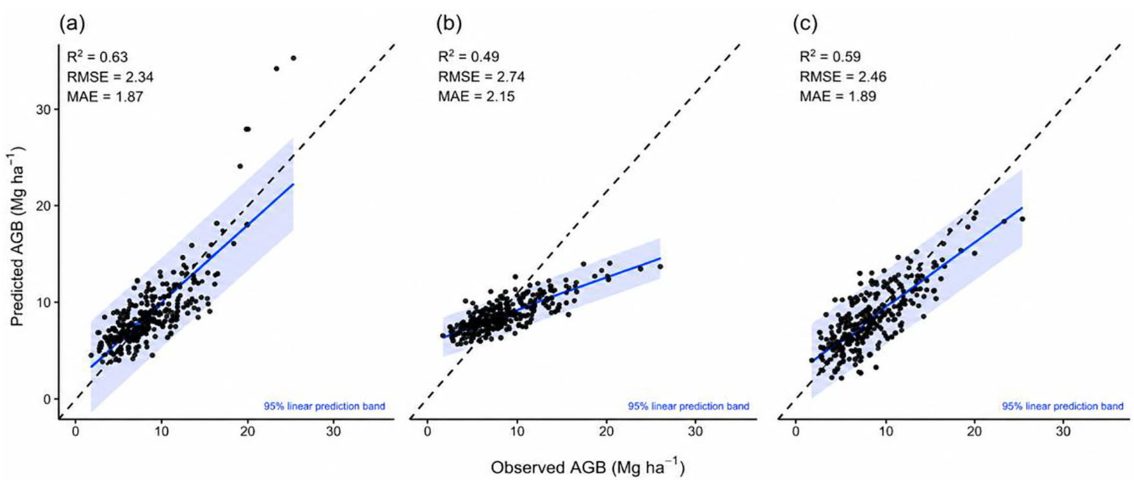

FIGURE 5
Observed versus predicted aboveground biomass under leave-one-paddock-out validation for GAMLSS, random forest, and radial support vector machine using the complete multisensor configuration (*n* = 280 held-out predictions per model). The dashed line represents the 1:1 relationship, the solid blue line represents the fitted observed–predicted relationship, and the shaded area represents its 95% confidence band.

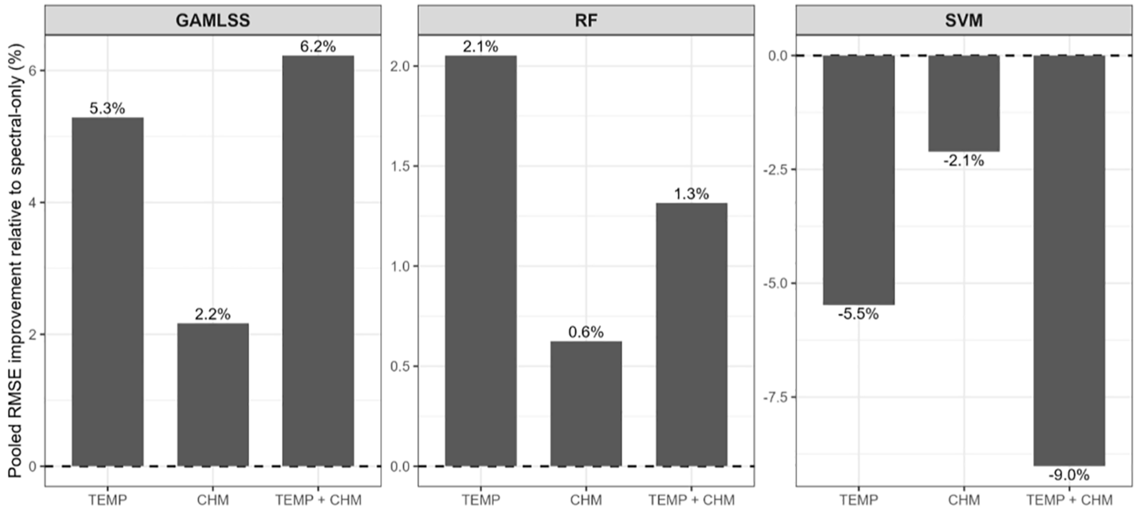

FIGURE 6
Contribution of canopy surface temperature (TEMP) and the canopy height model (CHM) to AGB prediction under leave-one-paddock-out validation. Positive values indicate RMSE reduction relative to the spectral-only configuration, whereas negative values indicate increased prediction error.

several portions of the paddock. The ICL paddocks showed relatively continuous zones of predicted biomass in some portions of the fields, whereas C6 displayed a more heterogeneous spatial distribution, including patches with comparatively lower predicted biomass and carbon stock. These contrasts are descriptive because no formal spatial or paddock-level statistical comparison was performed.

4 Discussion

4.1 Seasonal patterns in field and UAV-derived variables

The observed seasonal pattern is biologically consistent with the climatic seasonality of the Cerrado. Greater water availability and favorable growing conditions during the rainy season promote leaf expansion, tillering, photosynthetic activity, and biomass accumulation. In contrast, during the dry season, water deficit reduces leaf growth, accelerates senescence, and increases the presence of non-photosynthetically active material in the canopy, thereby reducing both canopy height and dry matter accumulation (Boukrouh et al., 2023). These ecophysiological responses help explain the lower AGB and canopy height observed during the dry season.

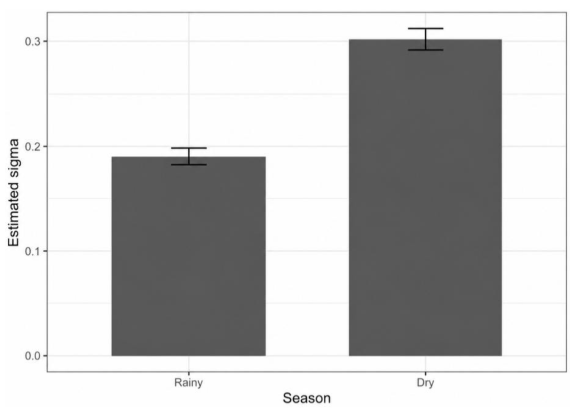

FIGURE 7
Season-specific dispersion parameter (σ) estimated by the final Gamma GAMLSS using the complete multisensor configuration. Bars represent mean estimates across resampling folds, and error bars represent the corresponding standard deviations. Higher σ values indicate greater conditional relative variability in AGB.

Comparable seasonal responses have been reported for tropical pastures in the Cerrado, where water availability strongly controls vegetation structure, biomass production, and spectral dynamics (Becerra et al., 2009; Meirelles et al., 2006; Santos et al., 2022, 2023). Boukrouh et al. (2023) also demonstrated that climatic and edaphic variability, including differences in precipitation, affected forage morpho-agronomic traits and dry matter production. Together, these findings indicate that the seasonal differences observed in the present study likely reflect the combined influence of water availability, pasture management, regrowth stage, and canopy architecture.

The spectral and thermal patterns are also consistent with the ecophysiological response of tropical grasses to seasonal water availability. During the rainy season, greater leaf water content, photosynthetic activity, and canopy development increase radiation scattering in the NIR while maintaining lower visible-band reflectance because of stronger pigment absorption. In contrast, dry-season water deficit accelerates leaf senescence, reduces leaf water content, and increases the proportion of dry vegetation, litter, and exposed soil. These changes increase visible-band reflectance, reduce the NIR response associated with vigorous vegetation, and promote greater canopy heating. This pattern appeared particularly pronounced in C6, where continuous grazing and greater soil exposure may have increased the contribution of dry litter and soil background to the spectral signal.

These findings agree with the principles described by Gausman et al. (1969), according to which visible reflectance is mainly controlled by pigment absorption, whereas NIR reflectance is strongly influenced by leaf internal structure and canopy

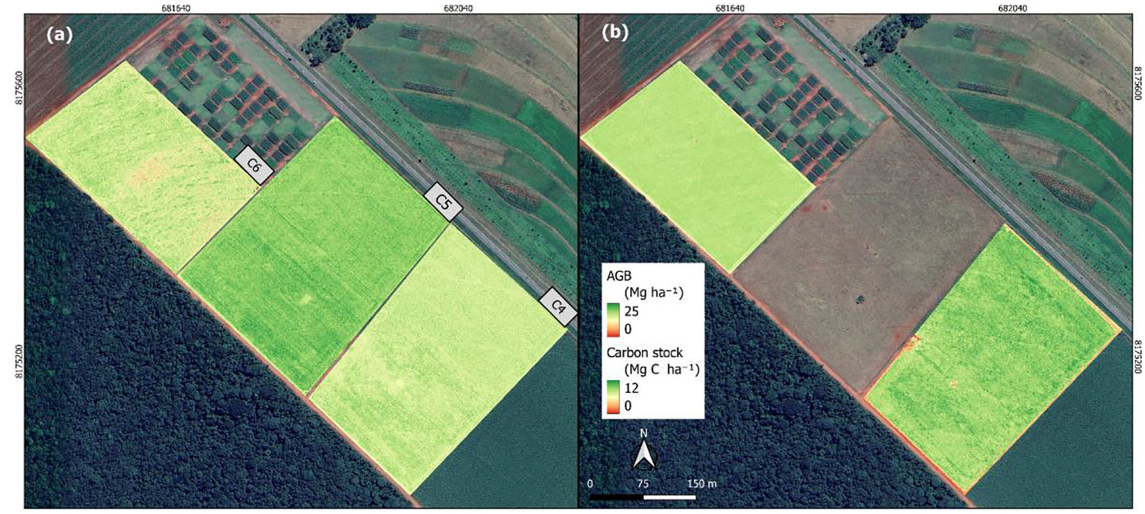

FIGURE 8
Spatial distribution of aboveground biomass (AGB) estimated using the GAMLSS model during the dry **(A)** and rainy season **(B)**, and biomass carbon stock of forage grass of the paddocks under integrated crop–livestock systems (C4 and C5) and under continuous pasture system (C6). In the rainy season **(B)**, the picture shows the C5 area under crop phase (rainfed rice at the harvest stage) of the integrated crop-livestock system. Crop phase was not part of the study.

organization. Studies conducted in Cerrado pastures have similarly shown that dry-season water deficit increases spectral mixing among green vegetation, non-photosynthetically active vegetation, and exposed soil, thereby reducing the stability of conventional optical indices (Becerra et al., 2009; Santana et al., 2017; Bretas et al., 2021; Silva et al., 2024). Consequently, integrating spectral, thermal, and structural information may improve the robustness of AGB estimation in heterogeneous tropical pastures (Alvarez-Mendoza et al., 2022; Bazzo et al., 2023).

4.2 Model performance, multisensor contributions, and seasonal dispersion

The results partially supported the hypothesis that thermal and structural variables would improve AGB prediction. Their contribution was positive for GAMLSS, modest for Random Forest, and negative for SVM. Although the isolated contribution of CHM to GAMLSS was modest, its inclusion provided complementary structural information for AGB estimation. This result is consistent with Batistoti et al. (2019), who demonstrated the usefulness of UAV photogrammetry-derived canopy height for estimating pasture biomass in the Brazilian Savanna. More broadly, Costa et al. (2021) showed that high-density UAV-LiDAR structural information can support aboveground biomass mapping across Cerrado vegetation. A recent study in wheat also supports the complementary contribution of spectral and structural UAV variables. Zhao et al. (2026) found that integrating canopy height with spectral information improved biomass estimation and that the relative contribution of these predictors varied across biomass levels, with canopy height becoming particularly informative at higher biomass levels. Although wheat differs from tropical pastures in canopy architecture and growth dynamics, these findings reinforce the complementary structural information provided by CHM in UAV-based biomass estimation.

The greater dry-season dispersion may reflect heterogeneous pasture responses to water limitation and grazing pressure. Differences among paddocks in senescence, residual green vegetation, litter accumulation, exposed soil, and regrowth stage may increase biomass variability during this period. By allowing dispersion to vary with season, GAMLSS directly represented part of this heterogeneity.

The favorable numerical performance of GAMLSS may therefore be related not only to its representation of nonlinear predictor–response relationships, but also to its ability to model both the conditional mean and season-dependent dispersion of AGB under a Gamma distribution. Cerrado pastures exhibit pronounced temporal and spatial heterogeneity associated with changes in canopy density, senescent material, soil exposure, and regrowth stage throughout the year (Bretas et al., 2021; Bazzo et al., 2023; Silva et al., 2024). These processes may generate asymmetric and heteroscedastic biomass distributions that are not fully described by models focused exclusively on conditional mean prediction. Random Forest and SVM can represent complex nonlinear relationships between predictors and AGB, which may explain their generally consistent predictive performance. For Random Forest, however, the contribution of additional predictor groups was not monotonic. The addition of thermal variables produced the largest reduction in RMSE, whereas the subsequent inclusion of CHM did not provide further improvement. This suggests that the structural information captured by CHM was only partially complementary to the spectral and thermal predictors in this dataset. However, their standard implementations do not explicitly parameterize season-dependent response dispersion in the same manner as the fitted GAMLSS model. Thus, the numerical advantage observed for GAMLSS in this dataset may be partly associated with its distributional representation of seasonal biomass variability.

The prediction errors obtained in the present study were within the broad range reported for pasture biomass estimation using remote-sensing data. Previous studies have shown that RF and SVM can provide useful biomass predictions in structurally heterogeneous pastures (Bispo et al., 2020; Alvarez-Mendoza et al., 2022). Studies using multispectral UAV or satellite data have also reported substantial variation in predictive accuracy depending on pasture type, biomass range, sensor configuration, sampling support, and validation design (Azubuike et al., 2025; Furnitto et al., 2026).

Direct numerical comparisons among studies should nevertheless be made cautiously because RMSE and MAE depend strongly on the biomass range, measurement units, field-sampling scale, and validation strategy. In particular, random observation-level validation primarily evaluates interpolation within the sampled system, whereas paddock-level exclusion provides a more demanding assessment of transferability among management units within the study site.

4.3 Spatial patterns of biomass and aboveground biomass carbon

The seasonal patterns shown in the maps were consistent with the differences observed in the field dataset. Greater water availability during the rainy season favours pasture growth and regrowth, whereas dry-season water limitation may restrict biomass accumulation and increase spatial heterogeneity. Nevertheless, the mapped contrasts may also reflect differences in grazing conditions, management history, regrowth stage, and campaign-specific environmental conditions.

The comparatively high predicted AGB and carbon stock observed in portions of C5 during the dry season may be associated with pasture regrowth and residual plant material following the crop phase. However, no formal analysis was conducted to isolate the effect of the production system from other differences among paddocks. Therefore, contrasts among C4, C5, and C6 should not be interpreted as direct evidence of greater biomass or carbon accumulation caused by integrated crop–livestock management. This cautious interpretation is also supported by recent evidence on carbon storage in Brazilian pasture-based systems. dos Santos et al. (2026) concluded that integrated systems do not inherently increase soil carbon stocks relative to pastures because their effects depend strongly on pasture management, soil fertility, nitrogen availability, and grazing intensity.

Although the present study evaluated standing aboveground biomass carbon rather than soil carbon, this evidence reinforces that differences among production systems should not be attributed solely to system configuration. Likewise, the more heterogeneous distribution observed in C6 may be related to differences in grazing pressure, canopy structure, forage regrowth, soil exposure, and vegetation vigour. Previous studies have reported that seasonal water stress and continuous grazing may reduce aboveground biomass and increase pasture heterogeneity, whereas integrated systems may improve vegetation cover and recovery (Batlle-Bayer et al., 2010; de Carvalho et al., 2023; Santos et al., 2023).

The spatial products should also be interpreted in light of their uncertainty. The maps represent conditional mean predictions and do not display pixel-level prediction uncertainty. Although GAMLSS allowed the calculation of distributional prediction intervals, these intervals were not spatially propagated. Likewise, the observed variability in carbon fraction (0.42 ± 0.01 g C g^{-1}) was not propagated to the spatial estimates because the mean value was applied uniformly. Seasonal and paddock-level differences in carbon fraction were not formally evaluated. Because the study included only palisade grass (Urochloa brizantha cv. BRS Paiaguás), variability among forage species could not be assessed.

The carbon estimates represent only the standing aboveground carbon contained in forage biomass at the time of each UAV survey, excluding roots, soil organic carbon, and other ecosystem carbon pools. They should not be interpreted as total ecosystem carbon stocks, net carbon sequestration, carbon-credit estimates, or temporal changes in carbon storage. Within these limitations, UAV-based mapping provides a useful representation of within-field variability, consistent with the application of UAV multispectral imagery for biomass and aboveground carbon mapping previously demonstrated by Lima et al. (2022) at the same experimental farm.

4.4 Applicability, transferability, and limitations

Overall, the results indicate the potential of multisensor UAV data combined with distributional regression for monitoring biomass variability within the evaluated experimental system. The complete multisensor GAMLSS configuration may support pasture monitoring and stocking-management assessments under conditions similar to those represented in the dataset. However, leave-one-paddock-out validation evaluates transfer among management units within the same experimental farm and should not be interpreted as external validation across independent farms, forage species, or biomes.

Accordingly, the findings should be regarded as a site-specific proof of concept. Broader operational application will require validation at independent farms, evaluation under additional environmental and management conditions, and explicit propagation of prediction uncertainty into the resulting spatial products.

5 Conclusions

This study showed that UAV-derived spectral, thermal, and structural information can be combined to estimate aboveground forage biomass under the heterogeneous and seasonally contrasting conditions of Cerrado pastures. However, the contribution of multisensor integration was model-dependent. The addition of canopy surface temperature and canopy height improved GAMLSS predictions, with the complete multisensor configuration reducing the leave-one-paddock-out RMSE by 6.2% relative to the spectral-only model. Random Forest showed smaller improvements, whereas the same predictor additions increased the prediction error of SVM. Therefore, the hypothesis that thermal and structural information would universally improve AGB prediction was only partially supported.

Among the evaluated approaches, GAMLSS produced the lowest numerical errors under both validation schemes. It achieved an R^2pred of 0.69 and an RMSE of 2.15 Mg ha^{-1} under repeated five-fold cross-validation, and an R^2pred of 0.63 and an RMSE of 2.34

Mg ha^{-1} under leave-one-paddock-out validation. Nevertheless, these differences should be interpreted as numerical rather than as evidence of statistically demonstrated superiority because no formal paired comparison of prediction errors was performed. Prediction accuracy decreased when complete paddocks were excluded, confirming that transfer to a management unit not represented during model fitting was more challenging than interpolation among observations from the sampled dataset.

The results also supported the use of a distributional regression framework. The GAMLSS formulation explicitly represented the greater conditional variability of AGB during the dry season, when the estimated dispersion parameter increased from approximately 0.19 in the rainy season to 0.30. The season-dependent dispersion model substantially improved model fit relative to the constant-dispersion formulation, indicating that seasonal differences in these pastures affected not only expected biomass but also its residual variability.

Seasonality was consistently reflected in field observations and UAV-derived variables. Rainy-season conditions were generally associated with greater biomass, canopy development, NIR and red-edge reflectance, whereas the dry season showed higher visible reflectance, canopy temperature, senescence, exposed soil and spectral–thermal heterogeneity. These responses demonstrate the relevance of combining complementary sensor information when monitoring tropical pastures affected by water limitation, grazing and variable regrowth conditions.

The resulting maps represented spatial variation in standing aboveground forage biomass and its corresponding biomass carbon at the dates of the UAV surveys. They should not be interpreted as estimates of total ecosystem carbon, net carbon sequestration, carbon credits, or evidence that integrated crop–livestock management directly caused greater carbon accumulation. The carbon estimates excluded roots, litter, soil organic carbon and other ecosystem pools, and uncertainty associated with model predictions and carbon concentration was not propagated spatially.

Overall, the study provides a site-specific proof of concept for combining multisensor UAV data with distributional regression to monitor forage biomass variability in Cerrado pastures. Leave-one-paddock-out validation demonstrated transferability among management paddocks within the same experimental farm, but not across independent farms, forage species, regions or biomes. Broader application will require external validation under additional environmental and management conditions, spatial propagation of prediction uncertainty, evaluation of temporal transferability and assessment of carbon-fraction variability. Within these limitations, the proposed approach should be interpreted as a site-specific proof of concept for field-scale pasture monitoring and as a basis for the development of more robust biomass and aboveground biomass-carbon assessment systems.

Data availability statement

The raw data supporting the conclusions of this article will be made available by the authors, without undue reservation.

Author contributions

GL: Conceptualization, Formal analysis, Investigation, Methodology, Software, Supervision, Validation, Visualization, Writing – original draft, Writing – review & editing. MF: Conceptualization, Investigation, Methodology, Supervision, Visualization, Writing – original draft, Writing – review & editing. LB: Data curation, Methodology, Software, Validation, Writing – original draft, Writing – review & editing. FF: Data curation, Investigation, Methodology, Supervision, Visualization, Writing – original draft, Writing – review & editing. PM: Conceptualization, Formal analysis, Funding acquisition, Project administration, Resources, Supervision, Writing – original draft, Writing – review & editing. AS: Investigation, Writing – original draft, Writing – review & editing. SK: Writing – original draft, Writing – review & editing. MAS: Funding acquisition, Project administration, Resources, Writing – original draft, Writing – review & editing. MC: Funding acquisition, Project administration, Resources, Writing – original draft, Writing – review & editing. MMS: Writing – original draft, Writing – review & editing. BM: Formal analysis, Funding acquisition, Investigation, Project administration, Resources, Supervision, Visualization, Writing – original draft, Writing – review & editing.

Funding

The author(s) declared that financial support was received for this work and/or its publication. This publication is based upon work supported by "Projeto Rural Sustentavel – Cerrado" in partnership with the Inter-American Development Bank (IDB), the UK Government, the Ministry of Agriculture of Brazil, the Brazilian Institute for Development and Sustainability (IABS), the ICLF Network Association and Embrapa via "IntegraC" project (Grant N° 20.18.03.043). The authors acknowledge the financial support through the partners of the Joint Call of the Cofund ERA-Net SusCrop (Grant N° 771134), FACCE ERA-GAS (Grant N° 696356), ICT-AGRI-FOOD (Grant N° 862665) and SusAn (Grant N° 696231) and to ERA-Net Cofund 2021 "SENSE" project (Grant N° 109), as well as funding by the New Zealand Government to support the objectives of the Global Research Alliance on Agricultural Greenhouse Gases (Grant N° 20.22.00.184). The authors acknowledge the contribution of Brazil's National Council for Scientific and Technological Development (CNPq) and the Coordination for the Improvement of Higher Education Personnel (CAPES) for the scholarship granted to GL (Grant No. 001). MF and BM are CNPq research fellows (Grant Nos. 317013/2023–8 and 311851/2026-6, respectively). We also acknowledge support from the National Institute of Science and Technology in Low Carbon Emission Agriculture (INCT-ABC), funded by CNPq (Grant No. 406635/2022-6), and from the Ministry of Agriculture (MAPA).

Conflict of interest

The author(s) declared that this work was conducted in the absence of any commercial or financial relationships that could be construed as a potential conflict of interest.

Generative AI statement

The author(s) declared that generative AI was not used in the creation of this manuscript.

Any alternative text (alt text) provided alongside figures in this article has been generated by Frontiers with the support of artificial intelligence and reasonable efforts have been made to ensure accuracy, including review by the authors wherever possible. If you identify any issues, please contact us.

Publisher's note

All claims expressed in this article are solely those of the authors and do not necessarily represent those of their affiliated organizations, or those of the publisher, the editors and the reviewers. Any product that may be evaluated in this article, or claim that may be made by its manufacturer, is not guaranteed or endorsed by the publisher.

References

Alvarez-Mendoza, C. I., Guzman, D., Casas, J., Bastidas, M., Polanco, J., Valencia-Ortiz, M., et al. (2022). Predictive modeling of above-ground biomass in Brachiaria pastures from satellite and UAV imagery using machine learning approaches. *Remote Sens.* 14, 5870. doi: 10.3390/rs14225870

Azubuike, B. N., Chlingaryan, A., Correa-Luna, M., Clark, C. E. F., and Garcia, S. C. (2025). Data augmentation and interpolation improves machine learning-based pasture biomass estimation from Sentinel-2 imagery. *Remote Sens.* 17, 3787. doi: 10.3390/rs17233787

Batistoti, J., Marcato Junior, J., Ítavo, L., Matsubara, E., Gomes, E., Oliveira, B., et al. (2019). Estimating pasture biomass and canopy height in Brazilian Savanna using UAV photogrammetry. *Remote Sens.* 11, 2447. doi: 10.3390/rs11202447

Batlle-Bayer, L., Batjes, N. H., and Bindraban, P. S. (2010). Changes in organic carbon stocks upon land use conversion in the Brazilian Cerrado: a review. *Agric. Ecosyst. Environ.* 137, 47–58. doi: 10.1016/j.agee.2010.02.003

Bazzo, C. O. G., Kamali, B., Hütt, C., Bareth, G., and Gaiser, T. (2023). A review of estimation methods for aboveground biomass in grasslands using UAV. *Remote Sens.* 15, 639. doi: 10.3390/rs15030639

Becerra, J. A. B., Shimabukuro, Y. E., and Alvalá, R. C. S. (2009). Relação do padrão sazonal da vegetação com a precipitação na região do Cerrado através de índices espectrais de vegetação. *Rev. Bras. Meteorol.* 24, 125–134. doi: 10.1590/S0102-77862009000200002

Bispo, P. D. C., Rodríguez-Veiga, P., Zimbres, B., do Couto de Miranda, S., Cezare, C. H. G., Fleming, S., et al. (2020). Woody aboveground biomass mapping of the Brazilian Savanna with a multi-sensor and machine learning approach. *Remote Sens.* 12, 2685. doi: 10.3390/rs12172685

Boukrouh, S., Bouazzaoui, Y., El Aich, A., Mahyou, H., Chikhaoui, M., Ait Lafkih, M., et al. (2024). Estimation of standing crop biomass in rangelands of the Middle Atlas mountains using remote sensing data. *Afr. J. Range Forage Sci.* 41, 244–259. doi: 10.2989/10220119.2024.2360991

Boukrouh, S., Noutfia, A., Moula, N., Avril, C., Louvieaux, J., Hornick, J. L., et al. (2023). Ecological, morpho-agronomical, and nutritional characteristics of Sulla flexuosa (L.) Medik. ecotypes. *Sci. Rep.* 13, 13300. doi: 10.1038/s41598-023-40148-y

Breiman, L. (2001). Random forests. *Mach. Learn.* 45, 5–32. doi: 10.1023/A:1010933404324

Bretas, I. L., Valente, D. S. M., Silva, F. F., Chizzotti, M. L., Paulino, M. F., D'Áurea, A. P., et al. (2021). Prediction of aboveground biomass and dry-matter content in Brachiaria pastures by combining meteorological data and satellite imagery. *Grass Forage Sci.* 76, 340–352. doi: 10.1111/gfs.12517

Broge, N. H., and Leblanc, E. (2001). Comparing prediction power and stability of broadband and hyperspectral vegetation indices for estimation of green leaf area index and canopy chlorophyll density. *Remote Sens. Environ.* 76, 156–172. doi: 10.1016/S0034-4257(00)00197-8

Cortes, C., and Vapnik, V. (1995). Support-vector networks. *Mach. Learn.* 20, 273–297. doi: 10.1007/BF00994018

Cortner, O., Garrett, R. D., Valentim, J. F., Ferreira, J., Niles, M. T., Reis, J., et al. (2019). Perceptions of integrated crop–livestock systems for sustainable intensification in the Brazilian Amazon. *Land Use Policy* 82, 841–853. doi: 10.1016/j.landusepol.2019.01.006

Costa, M., Silva, C. A., Broadbent, E. N., Leite, R. V., Mohan, M., Liesenberg, V., et al. (2021). Beyond trees: mapping total aboveground biomass density in the Brazilian savanna using high-density UAV-LiDAR data. *For. Ecol. Manage.* 491, 119155. doi: 10.1016/j.foreco.2021.119155

Dash, J., and Curran, P. J. (2004). The MERIS terrestrial chlorophyll index. *Int. J. Remote Sens.* 25, 5403–5413. doi: 10.1080/0143116042000274015

de Carvalho, A. M., de Jesus, D. R., de Sousa, T. R., Ramos, M. L. G., de Figueiredo, C. C., de Oliveira, A. D., et al. (2023). "Soil carbon stocks and greenhouse gas mitigation of agriculture in the Brazilian Cerrado—a review," in *Plants*, 12 (13), 2449. doi: 10.3390/plants12132449

dos Santos, R. A. F., Damian, J. M., Almagro, M., Santos, R. S., Frazão, L. A., Oliveira, D. M. S., et al. (2026). Understanding soil carbon storage mechanisms to support sustainable intensification of pasture-based livestock systems in Brazil. *Front. Sustain. Food. Syst.* 10, 1805905. doi: 10.3389/fsufs.2026.1805905

Escadafal, R., Belghith, A., and Ben Moussa, A. (1994). "Indices spectraux pour la télédétection de la dégradation des milieux naturels en Tunisie aride," in *Télédétection Et Dègradation Des Milieux Naturels En Tunisie Aride*. Eds. R. Escadafal, M. Pouget and M. C. Girard (ORSTOM, Paris), 253–259.

Fitzgerald, G. J., Rodriguez, D., Christensen, L. K., Belford, R., Sadras, V. O., and Clarke, T. R. (2006). Spectral and thermal sensing for nitrogen and water status in rainfed and irrigated wheat environments. *Precis. Agric.* 7, 233–248. doi: 10.1007/s11119-006-9011-z

Frame, J. (1981). "Herbage mass," in *Sward Measurement Handbook*. Eds. J. Hodgson, R. D. Baker and A. Davies (British Grassland Society, Berkshire), 39–67.

Furnitto, N., Failla, S. I. G., Sottosanti, G., Avondo, M., Bognanno, M., Biondi, L., et al. (2026). Remote sensing-based biomass assessment of Hedysarum coronarium from multispectral UAV imagery in a Mediterranean pasture. *Remote Sens.* 18, 1594. doi: 10.3390/rs18101594

Gausman, H. W., Allen, W. A., and Cardenas, R. (1969). Reflectance of cotton leaves and their structure. *Remote Sens. Environ.* 1, 19–22. doi: 10.1016/S0034-4257(69)90055-8

Gitelson, A. A. (2004). Wide dynamic range vegetation index for remote quantification of biophysical characteristics of vegetation. *J. Plant Physiol.* 161, 165–173. doi: 10.1078/0176-1617-01176

Gitelson, A. A., Gritz, Y., and Merzlyak, M. N. (2003). Relationships between leaf chlorophyll content and spectral reflectance and algorithms for non-destructive chlorophyll assessment in higher plant leaves. *J. Plant Physiol.* 160, 271–282. doi: 10.1078/0176-1617-00887

Gitelson, A. A., Kaufman, Y. J., and Merzlyak, M. N. (1996). Use of a green channel in remote sensing of global vegetation from EOS-MODIS. *Remote Sens. Environ.* 58, 289–298. doi: 10.1016/S0034-4257(96)00072-7

Gitelson, A. A., and Merzlyak, M. N. (1994). Spectral reflectance changes associated with autumn senescence of Aesculus hippocastanum L. and Acer platanoides L. leaves: spectral features and relation to chlorophyll estimation. *J. Plant Physiol.* 143, 286–292. doi: 10.1016/S0176-1617(11)81633-0

Gitelson, A. A., Stark, R., Grits, U., Rundquist, D., Kaufman, Y., and Derry, D. (2002). Vegetation and soil lines in visible spectral space: a concept and technique for remote estimation of vegetation fraction. *Int. J. Remote Sens.* 23, 2537–2562. doi: 10.1080/01431160110107806

Huete, A. A. (1988). A soil-adjusted vegetation index (SAVI). *Remote Sens. Environ.* 25, 295–309. doi: 10.1016/0034-4257(88)90106-X

Huete, A., Didan, K., Miura, T., Rodriguez, E. P., Gao, X., and Ferreira, L. G. (2002). Overview of the radiometric and biophysical performance of the MODIS vegetation indices. *Remote Sens. Environ.* 83, 195–213. doi: 10.1016/S0034-4257(02)00096-2

Hunt, E. R., Daughtry, C. S. T., Eitel, J. U. H., and Long, D. S. (2011). Remote sensing leaf chlorophyll content using a visible band index. *Agron. J.* 103, 1090–1099. doi: 10.2134/agronj2010.0395

Lima, G. S. A., Ferreira, M. E., Madari, B. E., and Carvalho, M. T. M. (2022). Carbon estimation in an integrated crop-livestock system with imaging sensors aboard unmanned aerial platforms. *Remote Sens. Appl. Soc Environ.* 28, 100867. doi: 10.1016/j.rsase.2022.100867

Louhaichi, M., Borman, M. M., and Johnson, D. E. (2001). Spatially located platform and aerial photography for documentation of grazing impacts on wheat. *Geocarto Int.* 16, 65–70. doi: 10.1080/10106040108542184

MAPA (2021). *Plano Setorial de Mitigação e Adaptação às Mudanças Climáticas para Consolidação de uma Economia de Baixa Emissão de Carbono na Agricultura—Plano ABC+* (Brasília: Ministério da Agricultura, Pecuária e Abastecimento).

MapBiomas (2025). Collection 10 of the Annual Land Cover and Land Use Maps of Brazil. Available online at: https://plataforma.brasil.mapbiomas.org/ (Accessed January 27, 2026).

Meirelles, M. L., Ferreira, E. A. B., and Franco, A. C. (2006). *Dinâmica sazonal do carbono em campo úmido do Cerrado. Documentos 164* (Planaltina, DF: Embrapa Cerrados).

Nelson, D. W., and Sommers, L. E. (1996). "Total carbon, organic carbon, and organic matter," in *Methods of Soil Analysis, Part 3: Chemical Methods*. Eds. D. L. Sparks, A. L. Page, P. A. Helmke, R. H. Loeppert, P. N. Soltanpour and M. A. Tabatabai (Soil Science Society of America, Madison, WI), 961–1010. doi: 10.2136/sssabookser5.3.c34

Oliveira, J. M., Gollany, H. T., Polumsky, R. W., Madari, B. E., Leite, L. F. C., Machado, P. L. O. A., et al. (2022). Predicting soil organic carbon dynamics of integrated crop–livestock system in Brazil using the CQESTR model. *Front. Environ. Sci.* 10, 826786. doi: 10.3389/fenvs.2022.826786

Oliveira, J. M., Madari, B. E., Carvalho, M. T. M., Assis, P. C. R., Silveira, A. L. R., Lima, M. L., et al. (2018). Integrated farming systems for improving soil carbon balance in the southern Amazon of Brazil. *Reg. Environ. Change* 18, 105–116. doi: 10.1007/s10113-017-1146-0

Pedreira, C. G. S., Silva, L. S., and Alonso, M. P. (2015). "Use of grazed pastures in the Brazilian livestock industry: a brief overview," in *Proceedings of the 1st International Conference on Forages in Warm Climates*. Eds. A. R. Evangelista, C. L. S. Avila, D. R. Casagrande, M. A. S. Lara and T. F. Bernardes (University of Lavras, Lavras), 11–20.

R Core Team (2025). *R: A Language and Environment for Statistical Computing* (Vienna: R Foundation for Statistical Computing). Available online at: https://www.R-project.org/ (Accessed August 14, 2026).

Reis, A. A., Werner, J. P. S., Silva, B. C., Figueiredo, G. K. D. A., Antunes, J. F. G., Esquerdo, J. C. D. M., et al. (2020). Monitoring pasture aboveground biomass and canopy height in an integrated crop–livestock system using textural information from PlanetScope imagery. *Remote Sens.* 12, 2534. doi: 10.3390/rs12162534

Rigby, R. A., and Stasinopoulos, D. M. (2005). Generalized additive models for location, scale and shape. *J. R. Stat. Soc Ser. C. Appl. Stat.* 54, 507–554. doi: 10.1111/j.1467-9876.2005.00510.x

Rouse, J. W., Haas, R. H., Schell, J. A., and Deering, D. W. (1974). "Monitoring vegetation systems in the Great Plains with ERTS," in *Proceedings of the Third Earth Resources Technology Satellite-1 Symposium, Washington, Dc, 10–14 December 1973. NASA SP-351* (National Aeronautics and Space Administration, Washington, DC), 309–317.

Santana, S. S., Brito, L. F., Azenha, M. V., Oliveira, A. A., Malheiros, E. B., Ruggieri, A. C., et al. (2017). Canopy characteristics and tillering dynamics of Marandu palisade grass pastures in the rainy–dry transition season. *Grass Forage Sci.* 72, 261–270. doi: 10.1111/gfs.12234

Santos, C. O., Pinto, A. S., Silva, J. R., Parente, L. L., Mesquita, V. V., Santos, M. P., et al. (2022). Assessing the wall-to-wall spatial and qualitative dynamics of the Brazilian pasturelands 2010–2018, based on the analysis of the Landsat data archive. *Remote Sens.* 14, 1024. doi: 10.3390/rs14041024

Santos, C. O., Pinto, A. S., Silva, J. R., Parente, L. L., Mesquita, V. V., Santos, M. P., et al. (2023). Monitoring of carbon stocks in pastures in the savannas of Brazil through ecosystem modeling on a regional scale. *Land* 12, 60. doi: 10.3390/land12010060

Silva, A. G. P., Galvão, L. S., Ferreira Júnior, L. G., Teles, N. M., Mesquita, V. V., and Haddad, I. (2024). Discrimination of degraded pastures in the Brazilian Cerrado using the PlanetScope SuperDove satellite constellation. *Remote Sens.* 16, 2256. doi: 10.3390/rs16132256

Vahidi, M., Shafian, S., Thomas, S., and Maguire, R. (2023). Pasture biomass estimation using ultra-high-resolution RGB UAV images and deep learning. *Remote Sens.* 15, 5714. doi: 10.3390/rs15245714

Vincini, M., Frazzi, E., and D'Alessio, P. (2008). A broad-band leaf chlorophyll vegetation index at the canopy scale. *Precis. Agric.* 9, 303–319. doi: 10.1007/s11119-008-9075-z

Woebbecke, D. M., Meyer, G. E., von Bargen, K., and Mortensen, D. A. (1995). Color indices for weed identification under various soil, residue, and lighting conditions. *Trans. ASAE* 38, 259–269. doi: 10.13031/2013.27838

Yang, Z., Willis, P., and Mueller, R. (2008). "Impact of band-ratio enhanced AWIFS image to crop classification accuracy," in *Proceedings of Pecora 17—the Future of Land Imaging… Going Operational* (American Society for Photogrammetry and Remote Sensing, Denver, CO).

Zhao, S., Luo, S., Fang, Z., Liu, X., and Chen, J. (2026). Multi dimensional variable influence mechanism analysis for wheat biomass estimation using fused UAV spectral and canopy height data and machine learning. *Front. Plant Sci.* 17, 1887967. doi: 10.3389/fpls.2026.1887967